Supporting Auxiliary Material

Assessment of cloud condensation nucleus activation of urban aerosol particles with different hygroscopic growth factors and the application to the cloud parcel model

Kaori Kawana[1], Naomi Kuba[2,3], and Michihiro Mochida[1]

[1]Graduate School of Environmental Studies, Nagoya University, Nagoya, Japan

[2] Research Institute for Global Change, Japan Agency for Marine-Earth Science and Technology, Yokohama, Japan

[3]Now also at: Atmosphere and Ocean Research Institute, the University of Tokyo, Kashiwa, Japan

Corresponding author: Michihiro Mochida, Department of Earth and Environmental Science, Graduate School of Environmental Studies, Nagoya University, Furo-cho, Chikusa-ku, Nagoya 464-8601, Japan. (mochida.michihiro@g.mbox.nagoya-u.ac.jp)

Reference

Drexler, R. R., and G. D. Rolph (2003), HYSPLIT (HYbrid Single-Particle Lagrangian Integrated Trajectory) Model access via NOAA ARL READY Website (http://www.arl.noaa.gov/ready/hysplit4.html), NOAA Air Resources Laboratory, Silver Spring, MD, USA

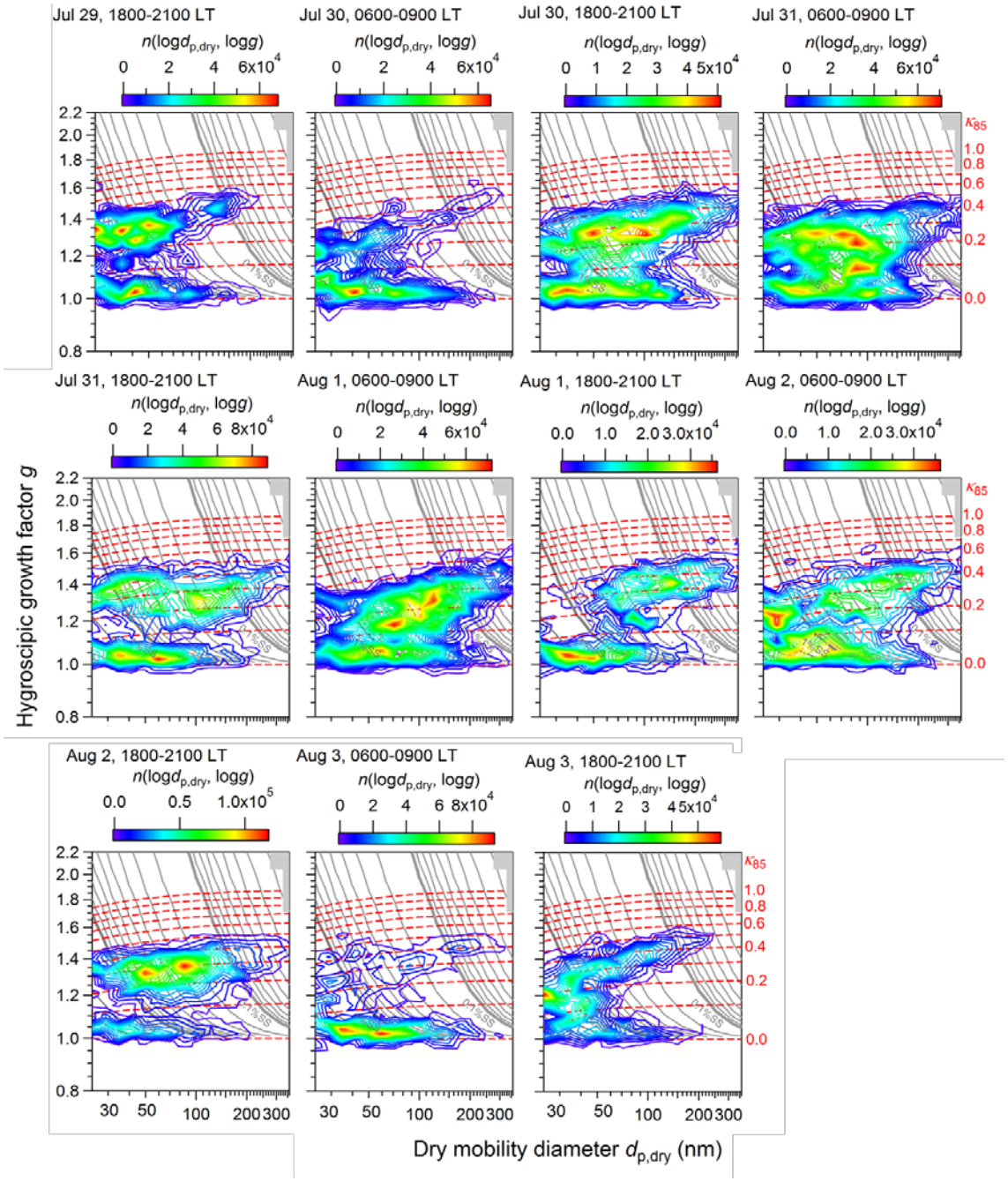

Figure S1. HTDMA-derived distributions of the aerosol particle number concentrations as a function of hygroscopic growth factor (g) and dry mobility diameter ($d_{p,dry}$) at 85% RH. The dashed red lines represent the contours of κ at 85% RH (κ_{85}). The gray contours show the critical supersaturation estimated from the κ-Köhler theory.

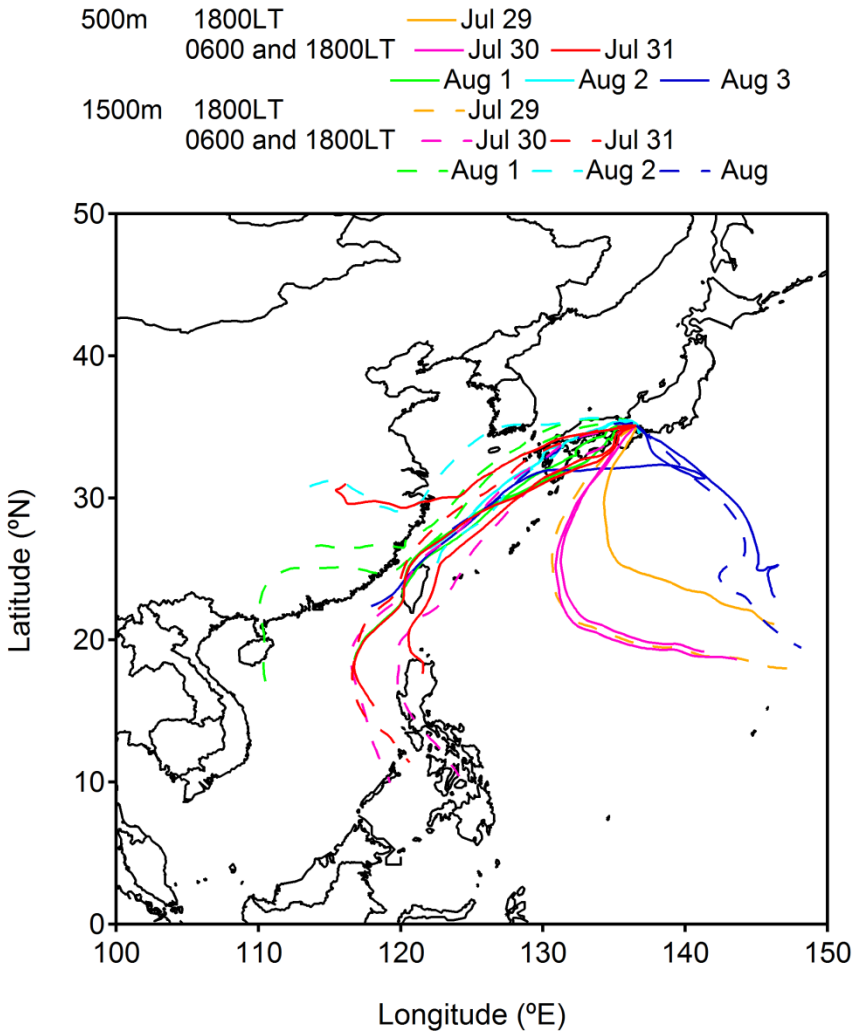

Figure S2. Five-day backward air mass trajectories from the observation site (500 and 1500 m above ground level) at 0600 and 1800 LT during the atmospheric observation period. The trajectory analysis was performed using the HYbrid Single-Particle Lagrangian Integrated Trajectory (HYSPLIT) model from the National Oceanic and Atmospheric Administration (NOAA) Air Resources Laboratory [*Draxler and Rolph*, 2003]. The meteorological data is from the Global Data Assimilation System (GDAS) of the National Centers for Environmental Prediction (NCEP). The solid and dashed lines represent the trajectories of air masses at 500 and 1500 m above ground level, respectively.

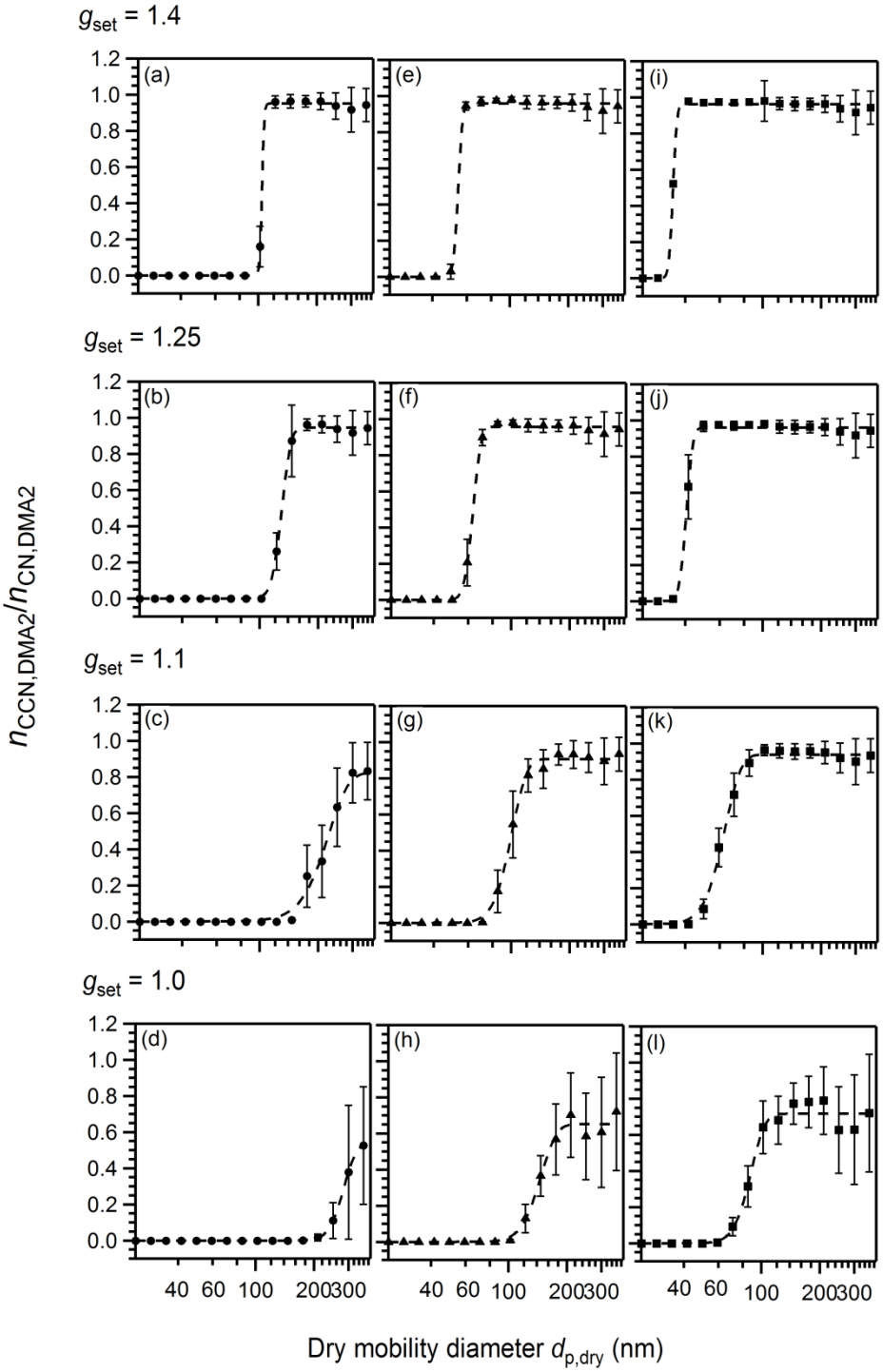

Figure S3. The averages of the predicted CCN efficiency spectra (symbols) and the curves fitted to the averages (dashed lines) for aerosol particles with g_{set} of (a, e, and i) 1.4, (b, f, and j) 1.25, (c, g, and k) 1.1, and (d, h, and l) 1.0 at (a–d) 0.18%, (e–h) 0.49%, and (i–l) 0.95% SS. The bars represent the standard deviation.

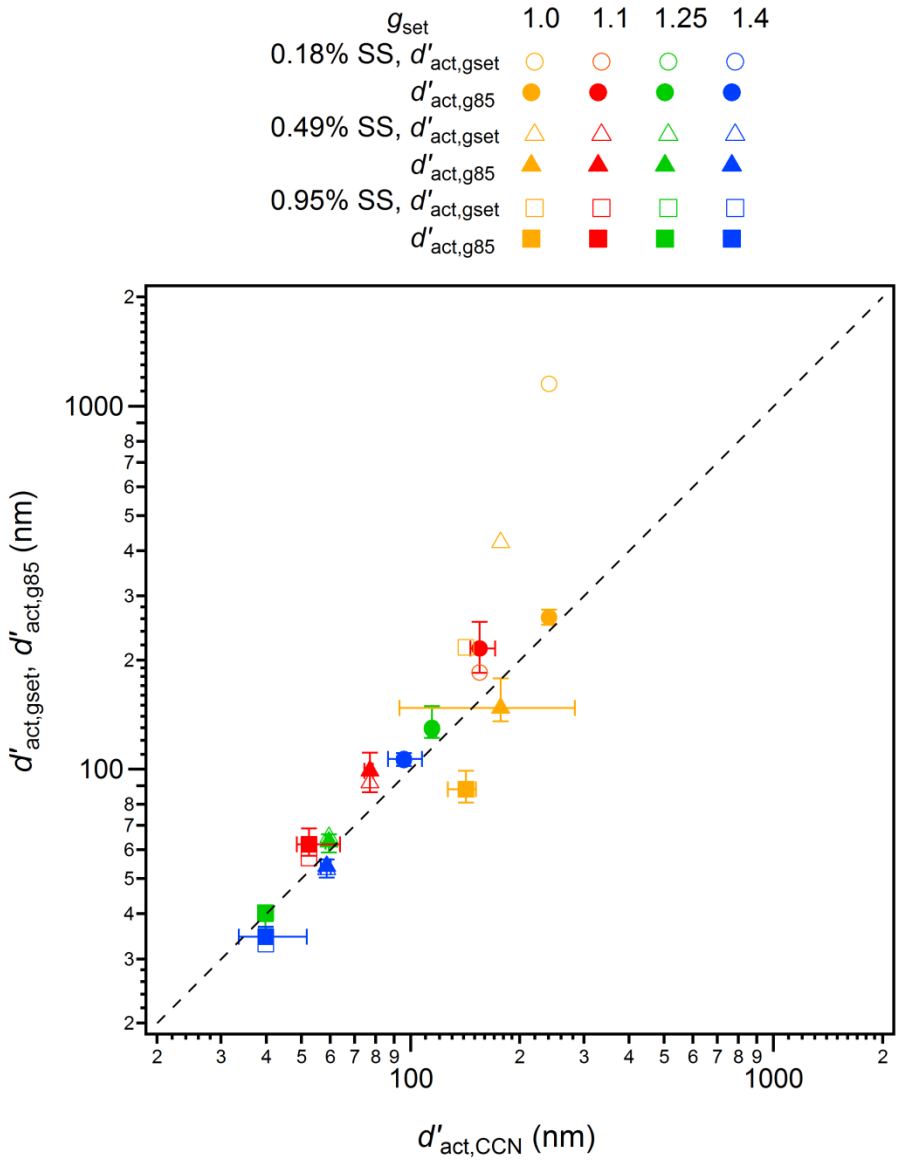

Figure S4. The relation between the predicted and measured CCN activation diameters obtained from the fittings to independent predicted CCN efficiency spectra (from 3-hour HTDMA data, see Figure S1) and independent measured CCN efficiency spectra, respectively. $d'_{act,g85}$ and $d'_{act,gset}$ are the averages of CCN activation diameters predicted from g_{set} with and without consideration of the width of the transfer function of DMA1, respectively, and $d'_{act,CCN}$ is the measured CCN activation diameters. The markers and bars represent the mean and standard deviation, respectively.

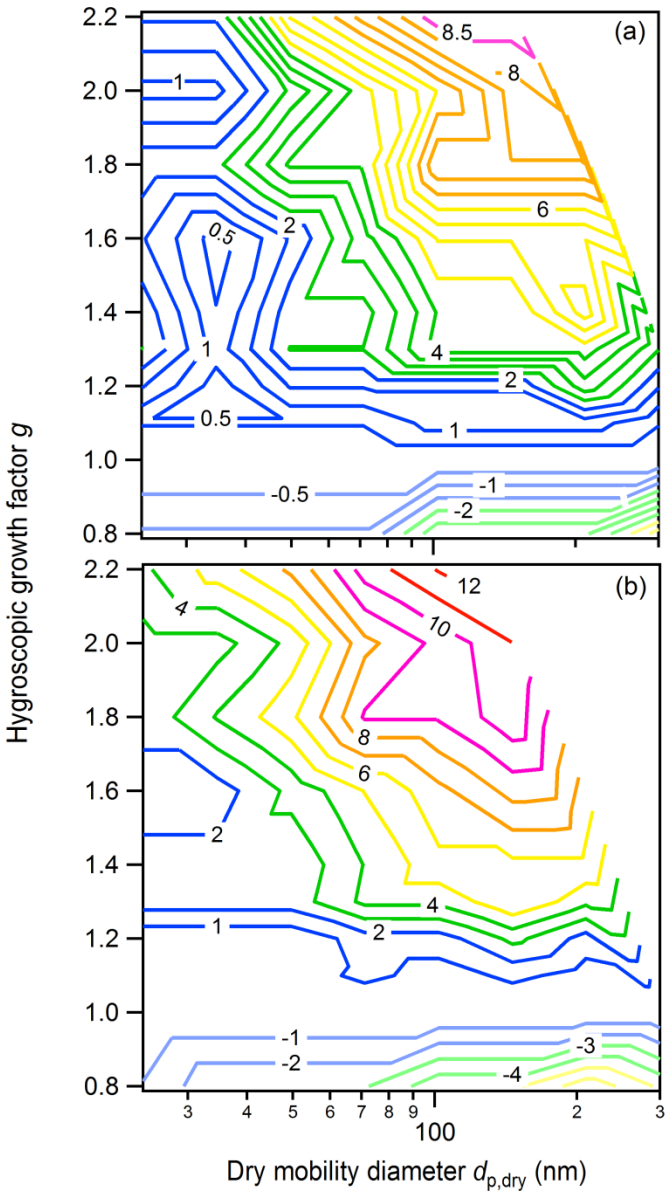

Figure S5. The differences of *g* of (a) doubly and (b) triply charged particles from those of singly charged particles with the same electrical mobility (in %). For multiply charged particles, the horizontal axis represents the dry mobility diameter ($d_{p,dry}$) of singly charged particles with the same mobility. The concept of the contour plots follows from *Duplissy et al.* [2009].

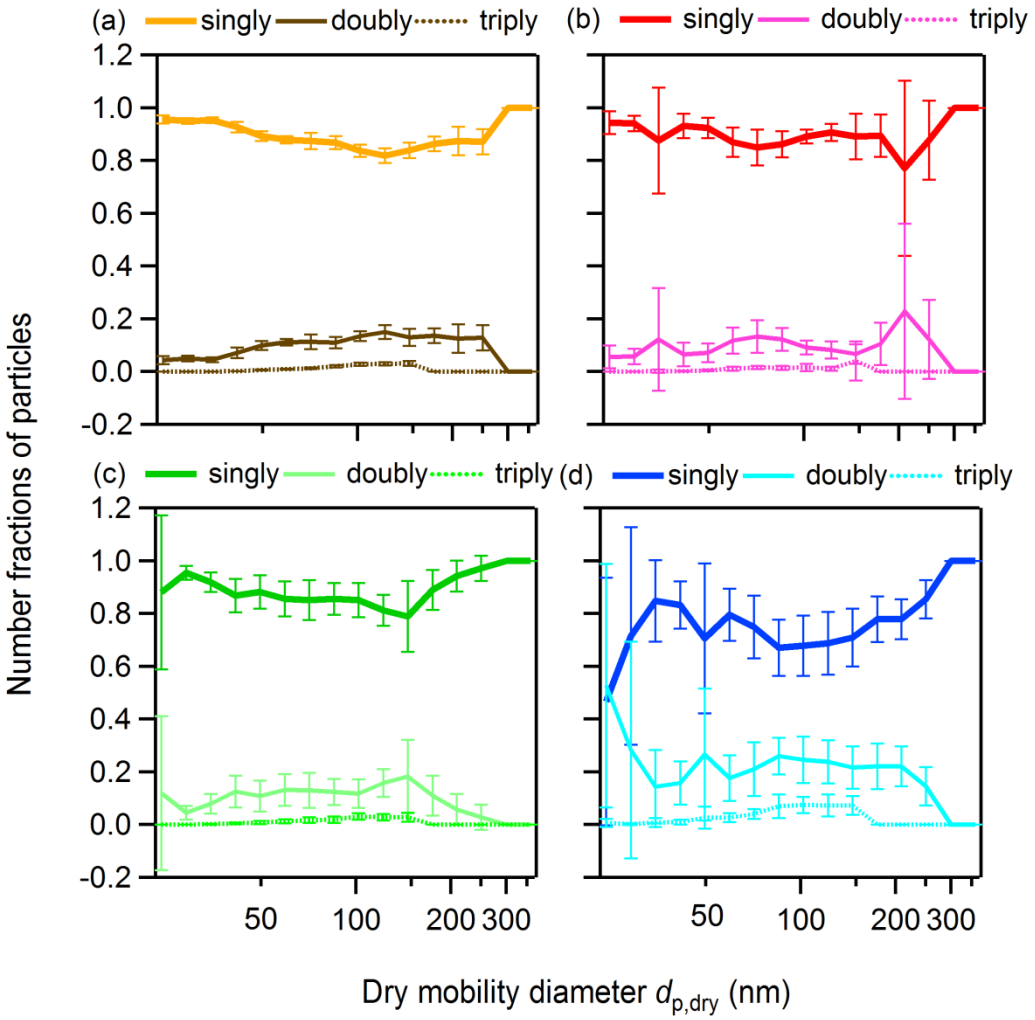

Figure S6. The estimated number fractions of singly, doubly, and triply charged particles among these particles in the ranges of (a) $0.8 \leq g < 1.1$, (b) $1.1 \leq g < 1.25$, (c) $1.25 \leq g < 1.4$, and (d) $1.4 \leq g \leq 2.2$. For doubly and triply charged particles, the horizontal axis represents the dry mobility diameter ($d_{p,dry}$) of singly charged particles with the same mobility.

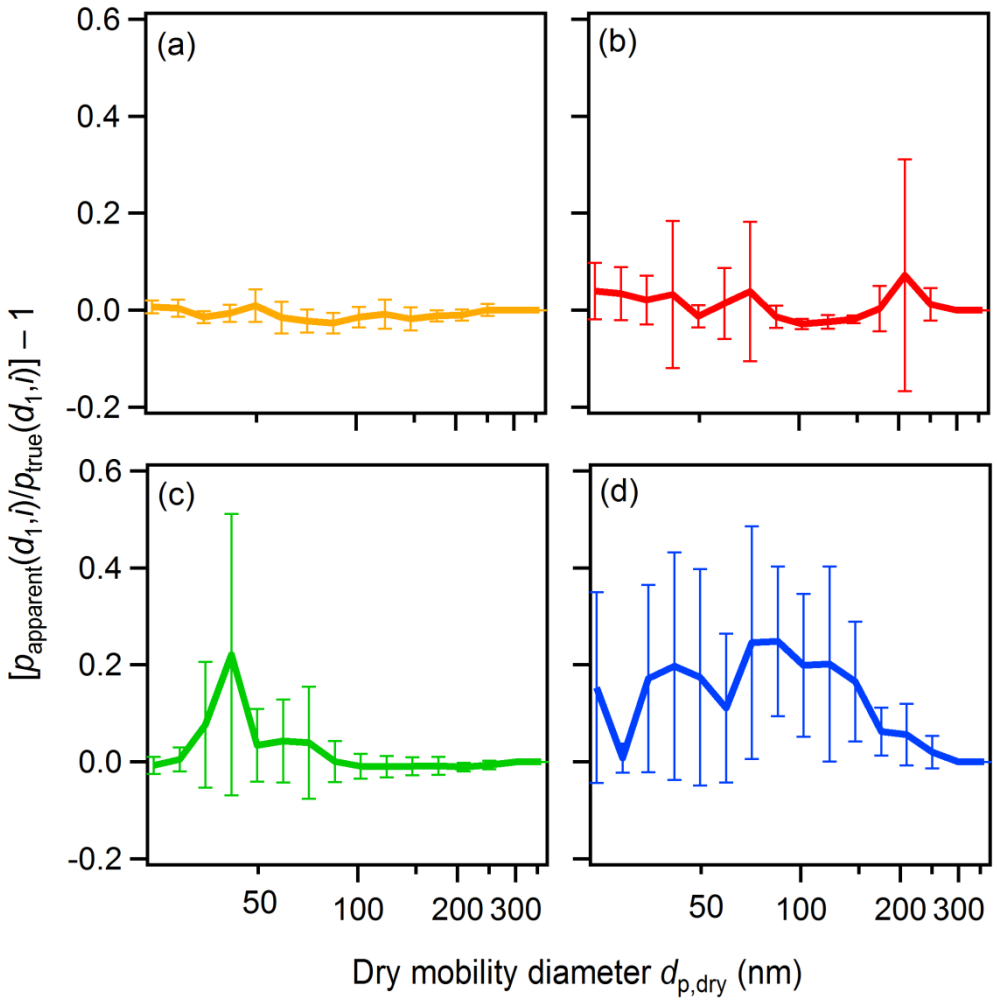

Figure S7. The estimated biases of the apparent probabilities of the presence of doubly and triply charged particles for particles in the ranges of (a) $0.8 \leq g < 1.1$, (b) $1.1 \leq g < 1.25$, (c) $1.25 \leq g < 1.4$, and (d) $1.4 \leq g \leq 2.2$ (see Appendix A1 for detail).

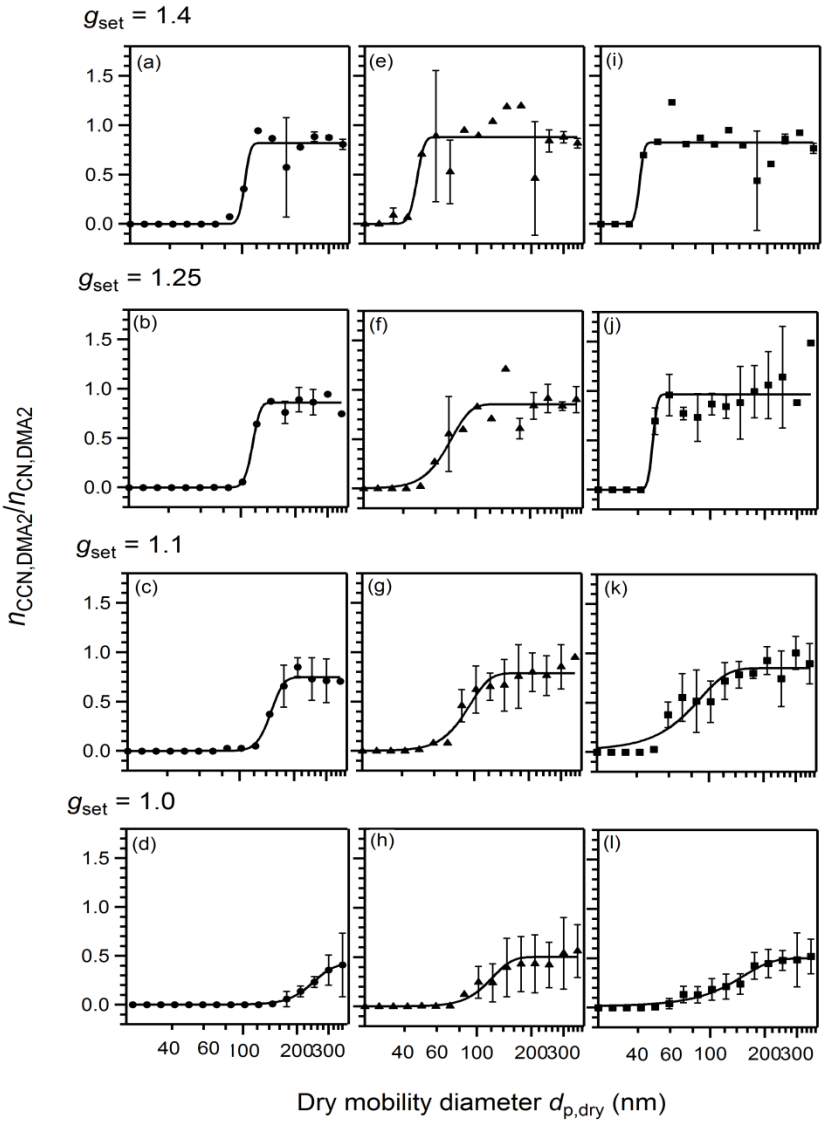

Figure S8. The averages of the measured CCN efficiency spectra (symbols) and the curves fitted to the averages (solid lines) for aerosol particles with g_{set} of (a, e, and i) 1.4, (b, f, and j) 1.25, (c, g, and k) 1.1, and (d, h, and l) 1.0 at (a–d) 0.18%, (e–h) 0.49%, and (i–l) 0.95% SS. The calculation is performed with consideration of $n_{CCN,DMA2}/n_{CN,DMA2}$ of doubly and triply charged particles sequentially from large to small diameters (see Appendix A1 for detail). The data points with negative values of $n_{CCN,DMA2}$ after correction of doubly and triply charged particles are omitted. Some data points are obtained from single samples as a result of the omissions. The standard deviation for data points from three or more samples are shown by bars.